REPORT DOCUMENTATION PAGE

Form Approved
OMB No. 0704-0188

1. REPORT DATE *(DD-MM-YYYY)*	2. REPORT TYPE	3. DATES COVERED *(From - To)*
Feb.28-2007	Final Report	June.1,2003-Nov.30,2006

4. TITLE AND SUBTITLE
Large Volume Non-Equilibrium Air Plasma at Atmospheric Pressure:A Novel Method with Low Power Requirements

5a. CONTRACT NUMBER

5b. GRANT NUMBER
F49620-03-1-0325

5c. PROGRAM ELEMENT NUMBER

6. AUTHOR(S)
Dr. Mounir Laroussi

5d. PROJECT NUMBER

5e. TASK NUMBER

5f. WORK UNIT NUMBER

7. PERFORMING ORGANIZATION NAME(S) AND ADDRESS(ES)
Old Dominion University

ODURF
4807 Hampton Blvd., Suite 2033
Hughes Hall,Old Dominion Univ.
Norfolk, VA 23529

8. PERFORMING ORGANIZATION REPORT NUMBER

9. SPONSORING / MONITORING AGENCY NAME(S) AND ADDRESS(ES)
Air Force Office
Of Scientific Research
875 North Randolph St.
Suite 325, Rm.3112
Arlington, VA, 22203-1768

Dr Robert Barker/NE

10. SPONSOR/MONITOR'S ACRONYM(S)
AFOSR

11. SPONSOR/MONITOR'S REPORT NUMBER(S)

12. DISTRIBUTION / AVAILABILITY STATEMENT
Unlimited

AFRL-SR-AR-TR-07-0341

13. SUPPLEMENTARY NOTES

14. ABSTRACT

This document is the final technical report on the research activities carried out under AFOSR Grant F49620-03-1-0325. Here we present our research results, which took place in the last three years and a half. Particularly, during the later period of performance the focus of our activities was on carrying out diagnostics on plasma devices based on new approaches that use high voltage narrow pulses to ignite the plasma. These novel approaches allow for the generation of non-thermal high-pressure discharges that can be used as radiation sources and for biomedical applications.

15. SUBJECT TERMS
Glow discharge, Atmospheric pressure, air plasma, current, non-equilibrium, pulsed plasma

16. SECURITY CLASSIFICATION OF:			17. LIMITATION OF ABSTRACT	18. NUMBER OF PAGES	19a. NAME OF RESPONSIBLE PERSON
a. REPORT	b. ABSTRACT	c. THIS PAGE			Dr. Robert J. Barker
Unclassified	Unclassified	Unclassified	Unlimited		19b. TELEPHONE NUMBER *(include area code)* (703) 696-8574

Final Report

Large Volume Non-Equilibrium Air Plasma at Atmospheric Pressure: A Novel Method with Low Power Requirements

AFOSR Grant F49620-03-1-0325

Prepared by

Dr. Mounir Laroussi. P.I.
Old Dominion University
Electrical & Computer Engineering Department
231 Kaufman Hall
Norfolk, VA 23529
Email: mlarouss@odu.edu

Submitted to

Dr. Robert J. Barker, Program Manager
Directorate of Physics and Electronics
Air Force Office of Scientific Research
875 North Randolph Street, Suite 325
Arlington, VA 22203

Period Covered: June 1, 2003 to November 30, 2006

Business Contact:

Mrs. Ruth Smith, Executive Director
Old Dominion University Research Foundation
4807 Hampton Blvd., Suite 2033
Hughes Hall
Norfolk, VA 23529
Email: rbsmith@odu.edu

Table of Contents

Abstract

This document is the final report, describing the research activities carried out under AFOSR Grant F49620-03-1-0325. Here we present the research results, which took place in the last three years and a half, under this program. Particularly, during the later period of performance the focus of our activities was on carrying out diagnostics on plasma devices based on new approaches that use high voltage narrow pulses to ignite the plasma. These novel approaches allow for the generation of non-thermal high-pressure discharges that can be used as radiation sources and for biomedical applications. In this document, descriptions of the new plasma devices and results from electrical and spectroscopic measurements are presented.

The work described in this report was carried out at the Applied Plasma Technology Laboratory of Old Dominion University, under the supervision of Dr. M. Laroussi, PI.

AC SYSTEM WITH WATER ELECTRODE

Recently, non-equilibrium atmospheric pressure plasmas have been used in a variety of material processing applications, biological and chemical decontamination of media, and the surface modifications of polymers. In the last decade, there has been considerable interest in finding methods for efficiently producing large volumes of such kinds of plasmas in air with free electron density greater than $10^{12}cm^{-3}$, at gas temperatures below 2000K.

Recently, we have been investigating a promising method whereby a stable, relatively large volume glow discharge in air can be generated with low input power and at relatively low gas temperature (below 2000K). This method is based on the application of an AC (60Hz) high voltage (<20Kv) to a pair of parallel electrodes separated by an air gap. One of the electrodes is a metal disc while the other electrode is a static or flowing volume of tap water (See Figure 1).

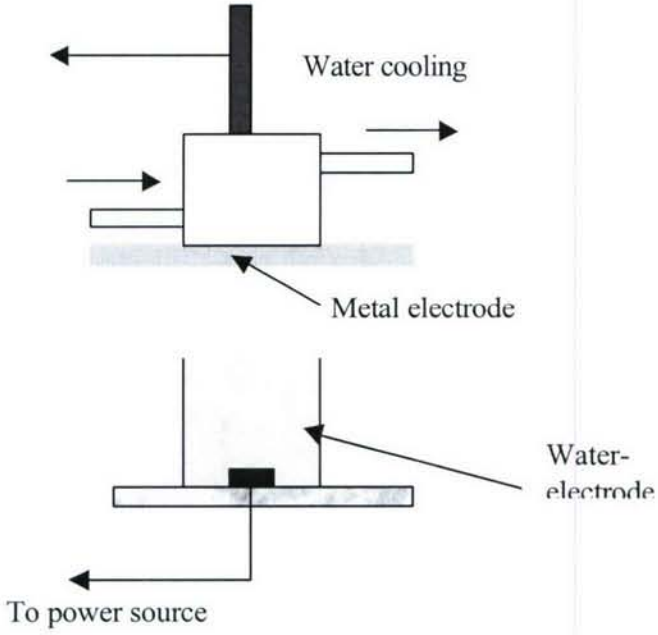

Fig. 1 Air Plasma Discharge Configuration

Figure 2 shows a photograph of the actual device. The upper electrode is a water-cooled stainless steel disk and the lower electrode is a slowly flowing water which emerges out of a glass tube positioned under the upper electrode at variable distances.

Fig. 2 Photograph of the experimental device. The plasma column in this picture is 1.3 cm long.

Current-Voltage Characteristics

The power supply is a high voltage transformer which is driven by a regulated 60 Hz AC voltage. The voltage across the electrodes was measured by means of a high voltage probe and an oscilloscope. The voltage across the secondary coil of the high voltage transformer without plasma is shown in Fig. 3, dashed line. When the secondary coil is connected to the plasma, the voltage across the plasma shows a rectangular shape, which is shown in Fig. 3, solid line. The voltage with plasma on can be considered to be appoximately constant during a half AC cycle. The rectangular shape of the voltage can be explained as follows: The secondary coil of the transformer has high internal impedance, which forms a voltage divider with the resistance of the plasma. An increase in voltage and current during a half AC cycle causes an increase in electron density in the plasma. Consequently the plasma conductivity increases and the resistivity decreases. A drop in the plasma series resistance leads to a drop in the voltage across it, which counteracts the increase in the total applied voltage. Most of the applied voltage actually shows up across the internal impedance of the power supply. Therefore the counteracting action of the discharge current and the plasma resistivity leads to an approximately constant voltage across the plasma. The discharge current was measured by a Pearson Coil placed around the lead of one of the electrodes. Figure 4 shows both the current and voltage waveforms.

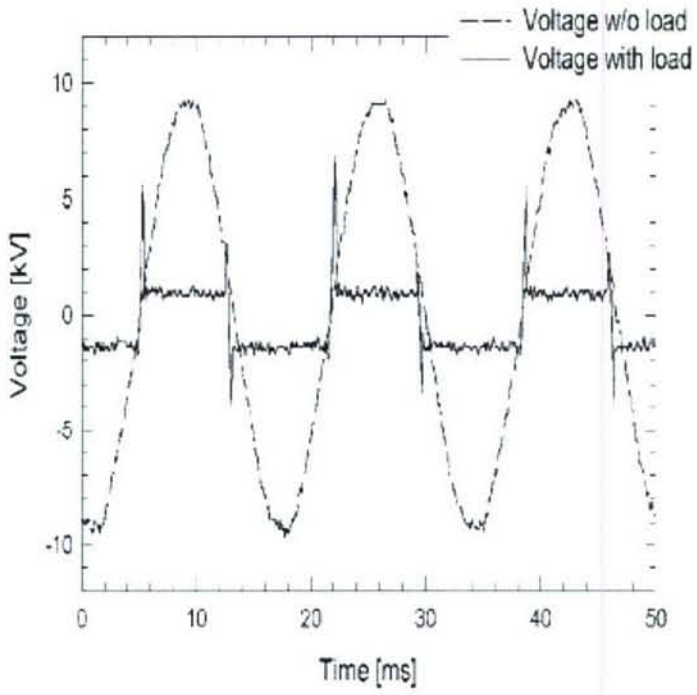

Fig. 3 Voltage across the electrodes, with and without plasma

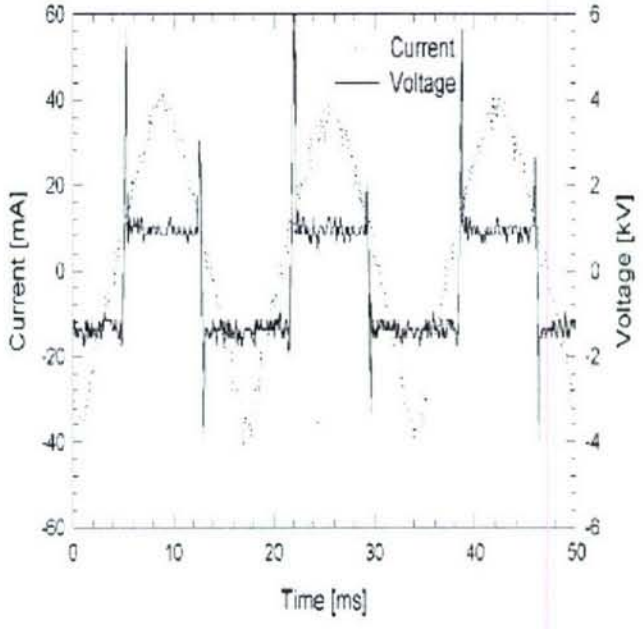

Fig. 4 Current and voltage waveforms

Plasma Diagnostics Results

A. Experimental Setup

Figure 5 shows the discharge apparatus and the various diagnostics instruments. The gap distance between the disk electrode and the surface of the water electrode is 1.3cm. The CCD camera (Stanford Computer Optics, Inc. Model 4 Picos, gating speed down to 200ps, adjustable in 100ps steps) can be triggered by either the signal from a current probe (Pearson Electronics Inc. Model 110A) or the light emission signal from the PMT (Acton Research Corp. Model R928, rise time 2.2ns). The plasma emission spectrum was measured by a spectrometer (Acton Research SpectraPro 500I, with 1200g/mm grating). The discharge current and the voltage across the two electrodes were measured by a current probe (Pearson Electronics Inc. Model 110A) and by a high voltage probe, repectively.

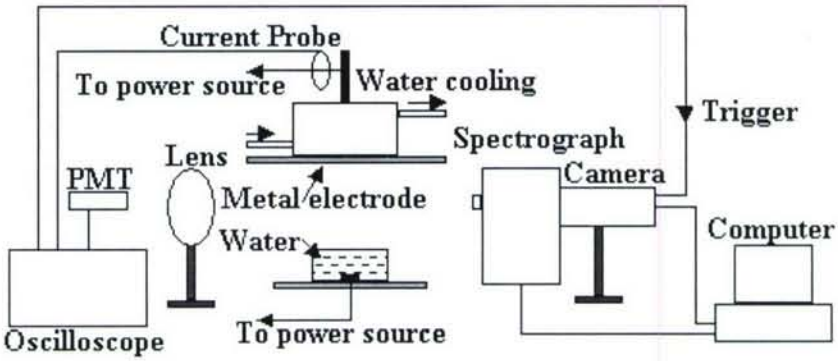

Fig. 5 Experimental setup

B. Determination of the plasma rotational and vibrational temperatures

To determine the rotational and vibrational temperatures, the simulated spectra of $C^3\Pi_u - B^3\Pi_g$ (Δv=-2) band transition of nitrogen are compared with the experimental results. The instrumental resolution is set to 0.22nm for this measurement. To make the comparison, all spectra (experimental and calculated) are normalized to the intensity of the (0-2) bandhead. First we determine the rotational temperature with the (0-2) band. Then we compare calculated spectra with the rotational temperature for various vibrational temperatures with experimental spectra. The result of the vibrational temperature is obtained when the best fit is achieved. Figure 6(a) shows the best fit of the calculated spectra and experimental spectra corresponding to the negative peak current. For comparison purposes, Fig. 6(b) and (c) show the calculated spectra for different rotational and vibrational temperatures. According to Fig. 6(a), the rotational temperature is 1800K. This temperature is about 20% higher than what we obtained from comparing the experimental and simulation spectra of 0-0 band of the second positive system of nitrogen. The vibrational temperature is about 2600K. According to Fig. 6(b) and (c), the accuracies of the rotational and vibrational temperatures are about 300K and 200K respectively.

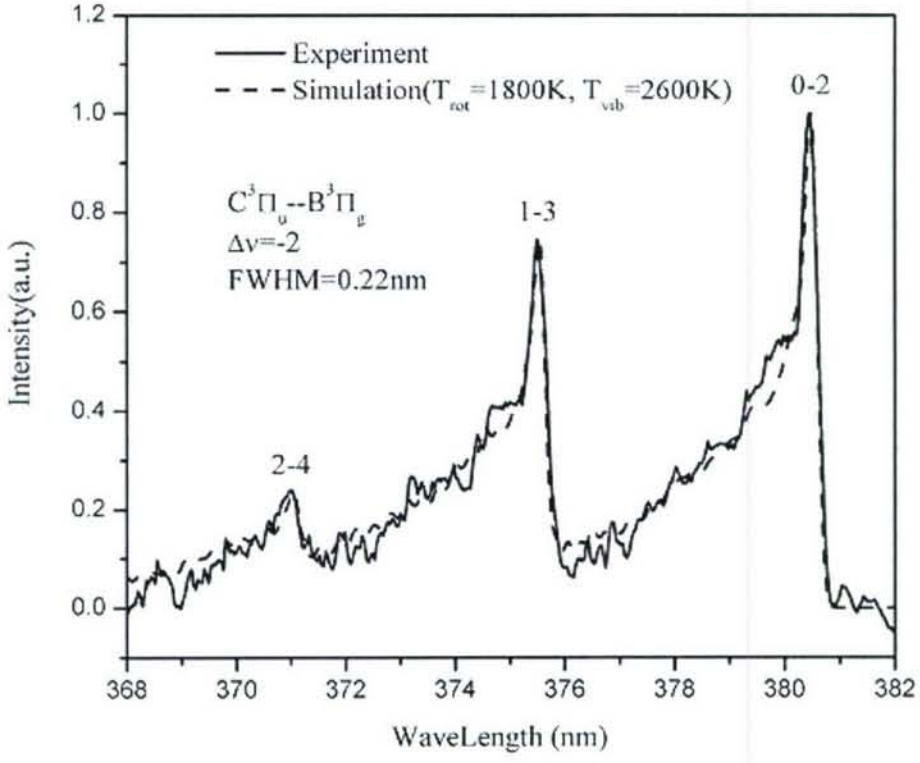

Fig 6a

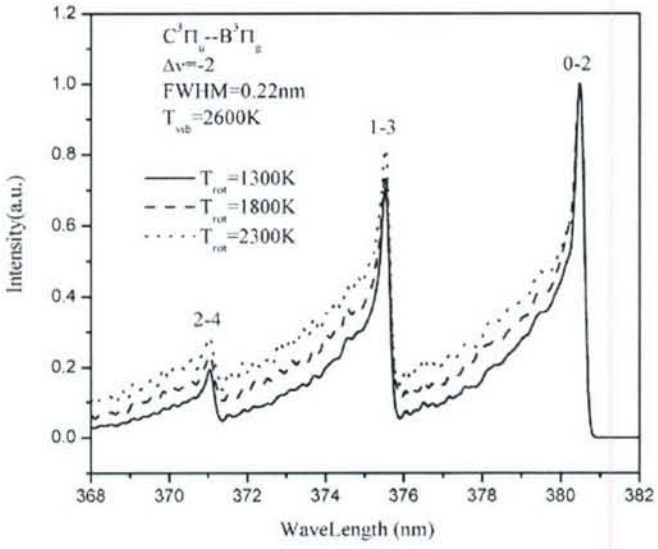

Fig. 6b

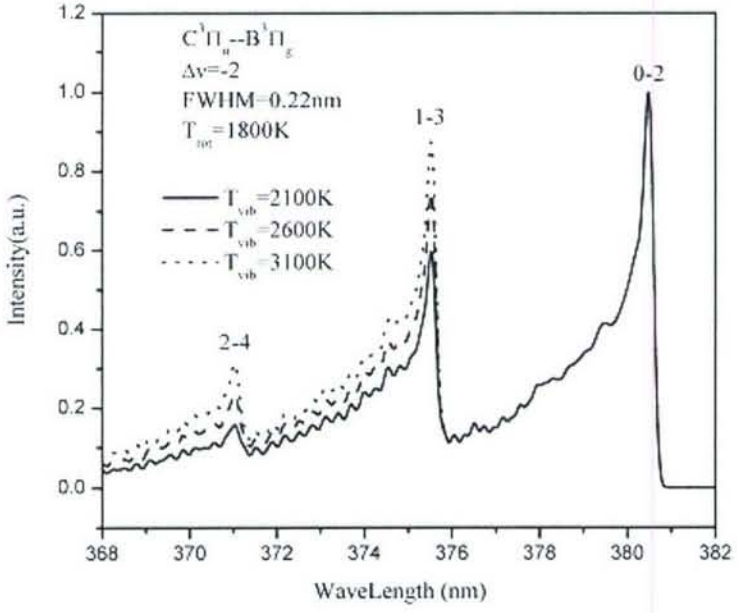

Fig. 6c

Fig. 6 Experimental and calculated spectra of the second positive system of nitrogen, Δv=-2 with FWHM 0.22nm for different rotational and vibrational temperatures. (a) best fit of experiment and simulation results, (b) simulation results with vibrational temperature 2600K and different rotational temperatures, and (c) simulation results with rotational temperature 1800K and different vibrational temperatures.

C. Temporal structure of the plasma

Figure 7 shows the current and light emission curves when the discharge is stable and the maximum available voltage is applied. When the current is positive, the water electrode actually plays the role of cathode. When the current is negative, it reaches a peak value that is higher than its positive peak value. Hence, the conductivity of the plasma during the half cycle when the water electrode is anode is higher than that when the water electrode is cathode. This is correlated by the fact that when the current is negative (water electrode is anode), the light emission intensity reaches a higher peak value than that when the current is positive. However, the light intensity peak is found to be delayed by about 0.6 ms with respect to the current peak (see Figure 7).

In order to characterize the temporal plasma structure, a high speed CCD camera is used to take pictures for different values of the discharge current. Figures 8(a) – (d) correspond to the times labeled 1 through 4 in Figure 7. The exposure time used to obtain the photos is 100μs. As can be seen in Figure 8(a), when the water electrode is cathode the plasma takes the shape of a relatively wide column (width of about 9 mm) but is not visually bright. In contrast, when the metal electrode is cathode, the plasma appears as a bright but narrow column (the plasma width shown in Figure 8(d) is about 5 mm). In addition, it can be seen from Figures 8(a) & (b) that when the water electrode is cathode, the plasma exhibits multi-contact points with the water surface. On the other hand, when the water electrode is anode, the plasma near the water surface becomes more uniform (Figures 8(c) & (d)).

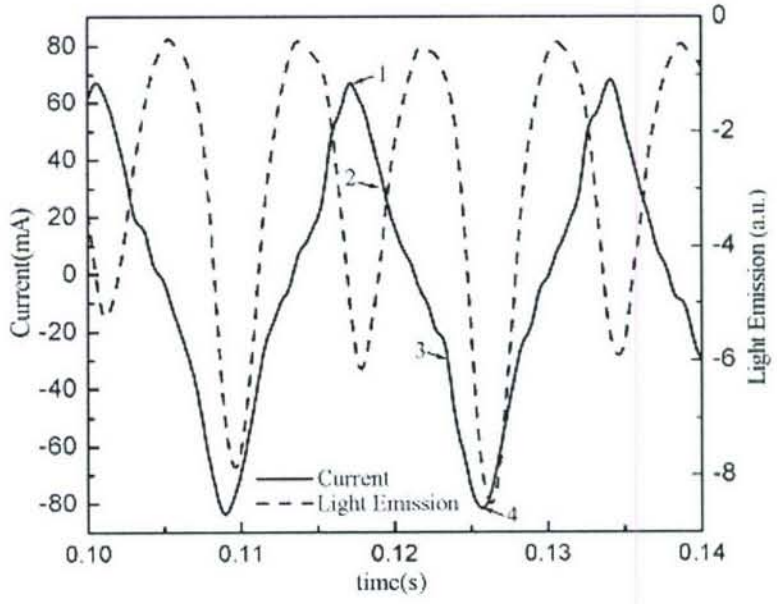

Fig. 7 Current and light emission curves when the discharge is stable. During the positive half cycle the water electrode is cathode; In the negative half cycle the water electrode is anode.

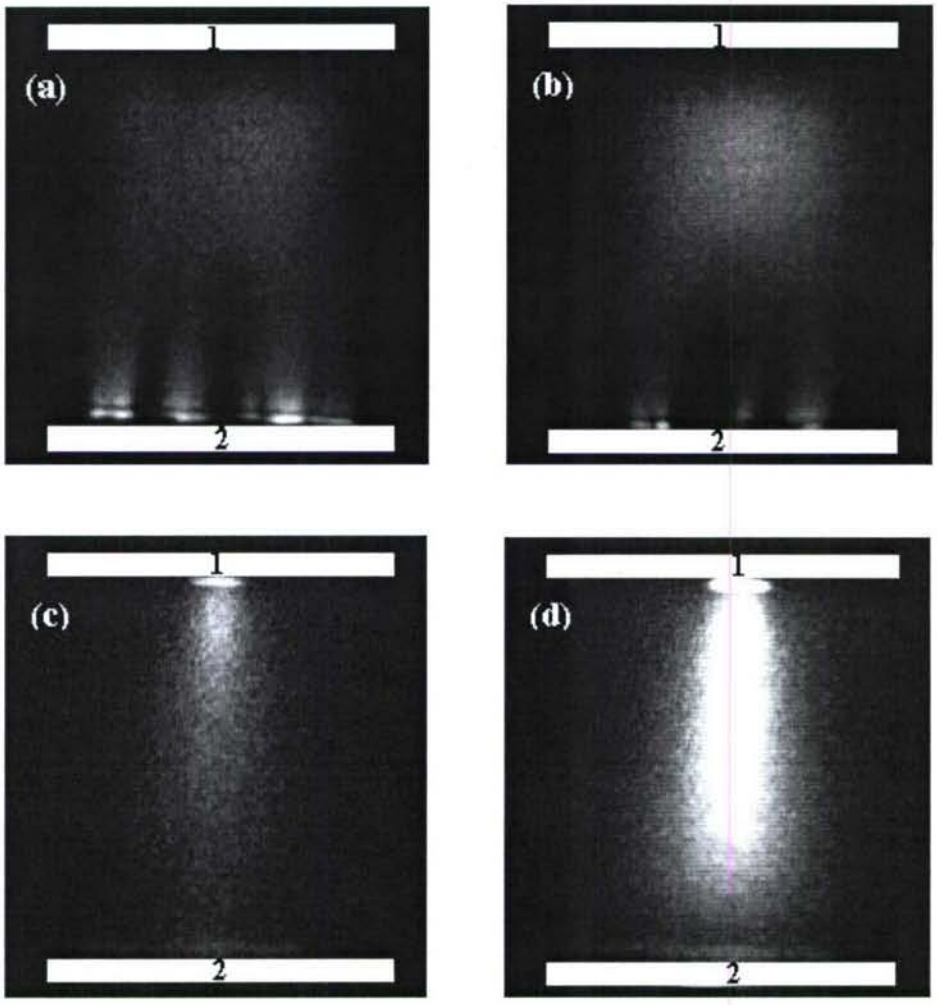

Fig. 8 Plasma photos. The top electrode, 1, is the metal electrode; the bottom electrode, 2, is the water electrode. Figures (a) – (d) correspond to the times labeled 1 through 4 in Figure 7. The exposure time is 100μs.

As mentioned earlier, the plasma exhibits different structures depending on the polarity of the water electrode. In order to capture photographically these structures, the applied voltage is slowly increased. When the voltage between the electrodes reaches about 12Kv (RMS), the air gap (1.3 cm in width) breakdown process is initiated. The discharge current is shown in Figure 9. The breakdown process begins with a small negative current peak. This is followed by larger fluctuations having higher peak values in the positive half-cycles. After 3 – 4 cycles, the current reaches a steady-state with a more symmetrical waveform. The breakdown occurs at the current sudden change point (point 1 as marked in Figure 9). In order to capture the initial process of breakdown, the high-speed CCD camera with an exposure time set at 5μs is used (below this value we obtain unclear images). Figures 10(a) & (b) show the pictures when the camera is triggered at the sudden change point 1 shown in Figure 9. Figure 10(a) clearly shows that the breakdown initiates from the water surface. Since the breakdown process occurs at very short

time scales, the smallest fluctuation in the trigger time results in the capture of the front-head of the discharge at different locations between the electrodes (Figures 10(a) and (b)). After the sudden change point, the current increases. The camera is then triggered at point 2 (see Figure 9). Figure 10(c) shows the picture of the discharge (taken at point 2) with an exposure time of 100 μs. Figure 10(d) shows another picture taken at point 1 but with an exposure time of 40μs. In this case, several discrete discharges originate from the water electrode. However, only one develops all the way to the metal electrode. For this exposure time (40 μs), the main discharge is found always to have already reached the metal electrode. Therefore, the speed of the discharge head must be much faster than 325 m/s. In fact, Figure 10(a) indicates that the velocity is close to 1000 m/s.

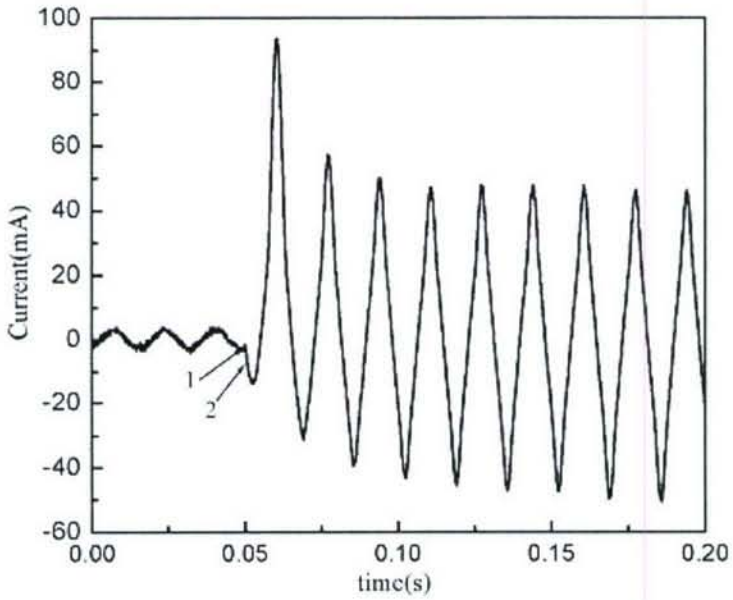

Fig. 9 Current waveform showing onset of the breakdown process

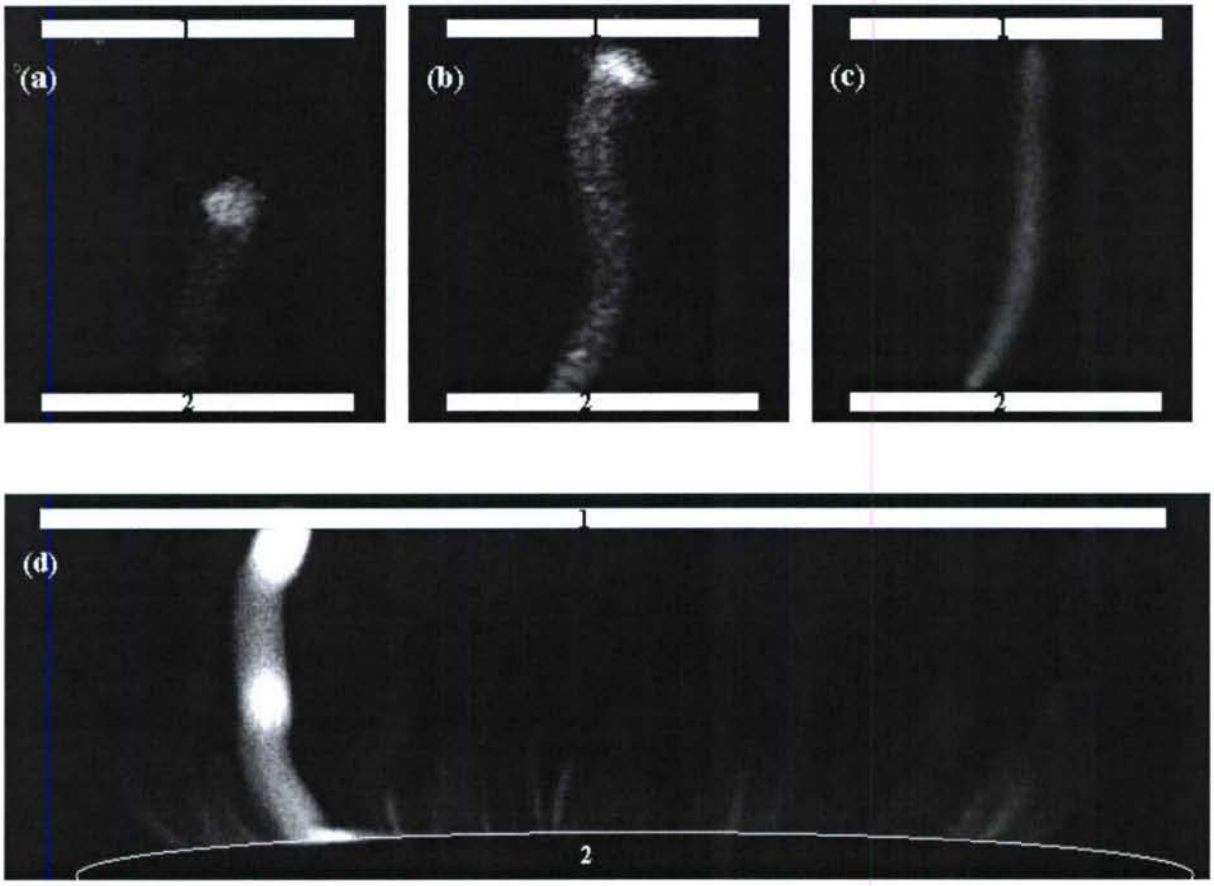

Fig. 10 High-speed picture of plasma ignition process. The top electrode 1 is the metal electrode and the bottom electrode 2 is the water electrode. The exposure times are: (a) and (b) 5μs, (c) 100μs, and (d) 40μs. Photos (a), (b) and (d) are taken at the sudden change point 1, and (c) at point 2 as shown in Figure 9.

As shown in Figures 8 (a) and (b) when the water electrode plays the role of cathode, the plasma has several discrete contact points with the surface of the water. This can be explained by the following experimental observation: Before breakdown is initiated, the water surface becomes clearly rippled. The peaks of the ripples offer sharp curvatures points playing the role of "pins". Several discharges can therefore be initiated at the head of the "pins", where high electric fields are present. In addition, Figures 8 (a)-(d) show that in the steady-state both the anode and the cathode have dark spaces associated with them along with a long bright column which occupies most of the gap space. These structures are consistent with the well-known structures of a normal glow discharge.

Figures 8 (c) and (d) show that when the water electrode is anode the multi-contact point feature is not present. This can be explained by the fact that the electric field near the water surface is not too high (most of the voltage drop is across the cathode fall, which in this case is near the metal electrode). Therefore the conditions are not suitable to sustain simultaneous discrete plasma ignition points at the water surface.

Figure 10(d) shows an example where there are three bright zones in the main discharge. The bright zone next to the metal electrode is the discharge head. Because the ion density is

higher than electron density in this area, the electric field in this area is high. The bright zones next to the water surface and in the middle are not well understood. In fact, sometimes there are two separate bright zones in the middle of the main discharge. This also needs further study.

D. Space and time-resolved band emissions

The hydroxyl radical plays an important role in biological and chemical decontamination processes. In order to determine the spatial distribution of the hydroxyl in the gap, a CCD camera (exposure time of 3μs) and 307.4 nm UV filter were used. Figures 11 shows a typical *OH* emission intensity distribution structure of the plasma when the current reaches its negative peak (water electrode is anode). The cathode fall region has a width of less than 0.2mm. The bright negative glow is next to it. The main part of the gap is occupied by the positive column. The dark zone close to water electrode (anode) is the anode dark space. These structures are consistent with the well-known structures of a normal glow discharge.

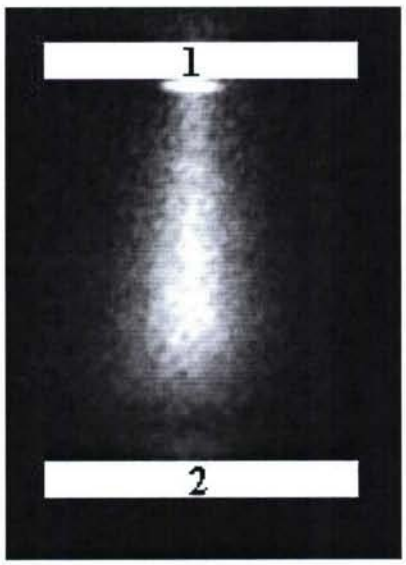

Fig. 11 Spatial distribution of the OH emission intensity. Exposure time: 3 μs

In order to know the temporal behavior of the emission intensities of OH, N_2, and N_2^+, the spectrometer is used. The instrumental resolution is set to 4nm (Full Width Half Maximum). A photomultiplier tube (Hamamatsu R928) (PMT) serves as detector. The output of the PMT is connected to a wide band oscilloscope. Figure 12 shows the temporal emission behavior of OH. The discharge current, N_2(C-B, 0-0 transition, 337nm), the combined emission of N_2 (C-B, 0-1 transition, 357.6nm) and N_2^+(B-X, 1-0 transition, 357.9nm) are also shown in Figure 12. The OH emission intensity doesn't depend on whether the current is positive or negative, but the N_2(C-B, 0-0), the sum of N_2(C-B, 0-1) and N_2^+(B-X, 1-0) emission intensities are stronger when the current is negative (water electrode is anode) than that when the current is positive (water electrode is cathode). As shown in Figure 12, the OH emission intensity stays relatively constant during most time of the discharge cycle and decreases quickly only when the current is close to zero. This shows that this source is an excellent source of the OH radical.

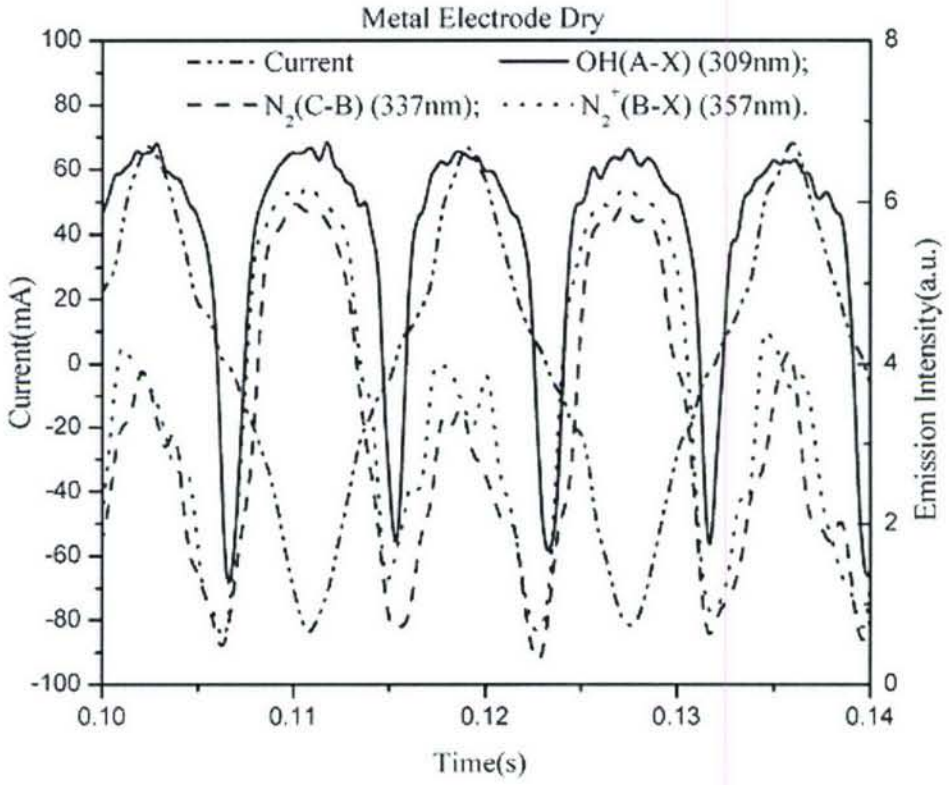

Fig. 12 The temporal behavior of emission intensities of OH(A-X, 0-0)(309nm), N_2(C-B, 0-0)(337nm), and the combined emissions of N_2(C-B, 0-1, 357.6nm) and N_2^+(B-X, 1-0, 357.9nm). The instrumental resolution is 4nm (Full Width at Half Maximum). The discharge current is also shown.

PULSED SYSTEMS

The electron energy distribution in non-equilibrium discharges plays the most important role in defining the chemistry in the plasma. It is through electron impact excitation and ionization that the charged particles, excited species, and radicals are produced. Increasing the electrons number density and their energy translates to an increase in the production of reactive species and UV radiation emission. To achieve this increase of ionization and to extend the electron energy distribution to higher values, short high voltage pulses will be used. Using short duration pulses has the advantages of keeping a low average power and not substantially increasing the gas temperature.

In this project we intend on using a repetitive pulse generator delivering up to 10 kV with a rise time of few nanoseconds to drive a Dielectric Barrier Discharge (DBD) in various gas mixtures, including air. Air plasma, for example, produces a variety of chemically reactive species such as O, OH, and NO, which play major roles in applications such chemical and biological decontamination. UV radiation is also generated by various atomic and molecular transitions such in N_2 and NO (NO_β).

A. Results from a Pulsed Dielectric Barrier Discharge

A Novel Discharge device:

Figure 13 shows the configuration of our pulsed DBD device. In this setup, one electrode is covered by a dielectric sheet and the second electrode is made of a copper disc with several holes for gas injection. The diameter of the copper disc is 5.7cm. The diameter of the holes is about 1mm. The distance between nearby holes is 5mm. The gap distance is adjustable from 1mm to centimeters range. The gas flows out of the holes and into the discharge gap. Relatively large volume diffuse plasmas at atmospheric pressure have been routinely generated by this device for various gas mixtures.

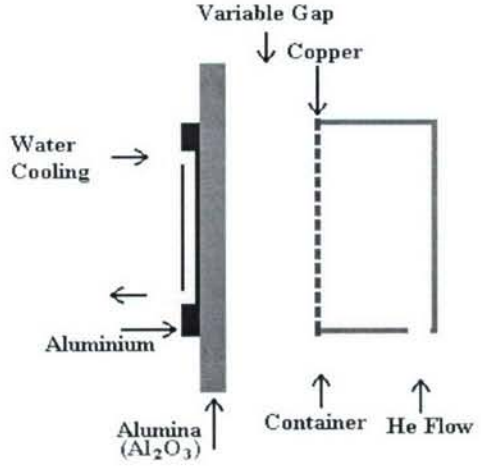

Fig. 13 Novel configuration of the DBD device

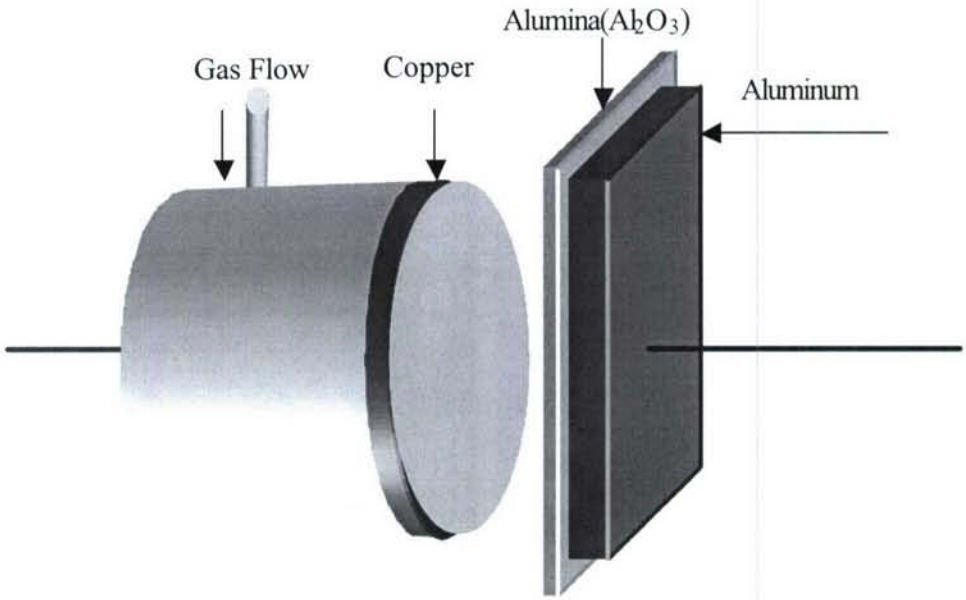

Fig. 14 A three-dimensional schematic of the discharge device

Power supply and electrical diagnostics

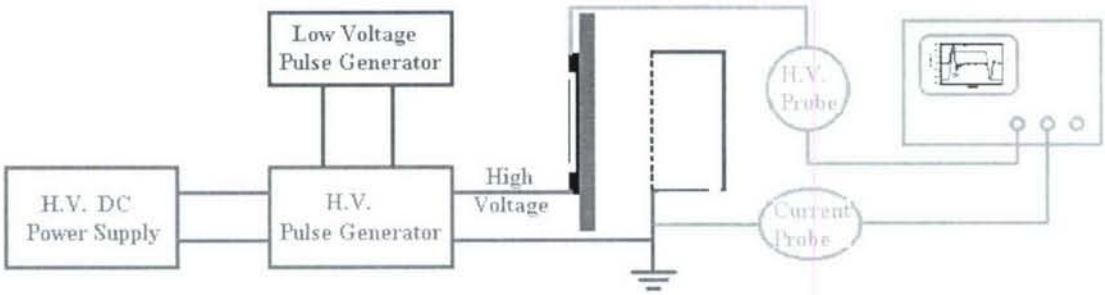

Fig. 15 Experimental set-up showing high voltage pulse generation, DBD, and Diagnostics System.

The parameters of the H.V. pulse output are:

- Repetition rate: 0-10kHz.
- Pulse width: 200ns to DC.
- Pulse amplitude: 0-10kV.
- Pulse rise and fall time: <60ns.

Electrical Diagnostics:

- Voltage is measured by Tektronix P6015A high voltage probe.
- Current is measured by Tektronix A6312 current probe.

Plasma structure and stability

Figure 16 shows a photograph of the plasma. The pulse frequency is 1kHz, the pulse width is 400ns, and the amplitude of the pulse is 8kV. The copper electrode (left) is grounded. The gap distance is 10mm, and the operating gas is a mixture of helium and air. As can be seen in the photo, diffuse and uniform plasma fills the entire volume between the electrodes. Intense visible light is emitted. The device can be operated for hours without overheating of the electrodes and without degradation of the plasma structure. In additions items exposed to the plasma do not undergo any visible damage and do not experience a substantial temperature rise.

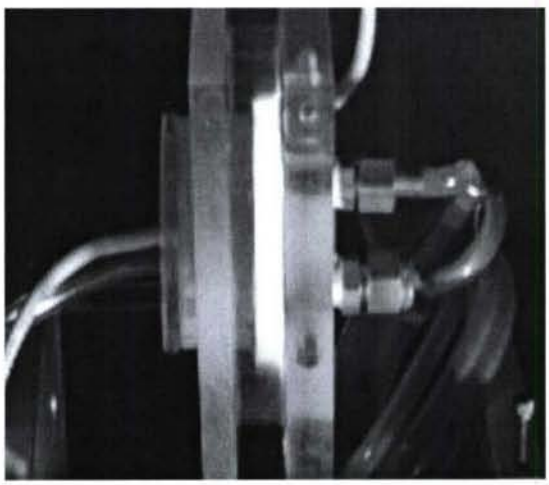

Fig. 16 Photo of the plasma. The gap distance is 10mm.

Current-voltage characteristics

Current measurements show two narrow current pulses, a positive one a short time after the voltage rising edge and a negative one at the falling edge of the voltage pulse. The negative current pulse is caused by the voltage induced by the charge accumulation on the dielectric during the first current pulse. These current pulses have peaks of few amperes and are about 100 ns wide.

The following I-V curves were obtained under the following conditions: The pulse frequency is 1kHZ, the pulse width is 400ns, and amplitude of the pulse is about 8kV.

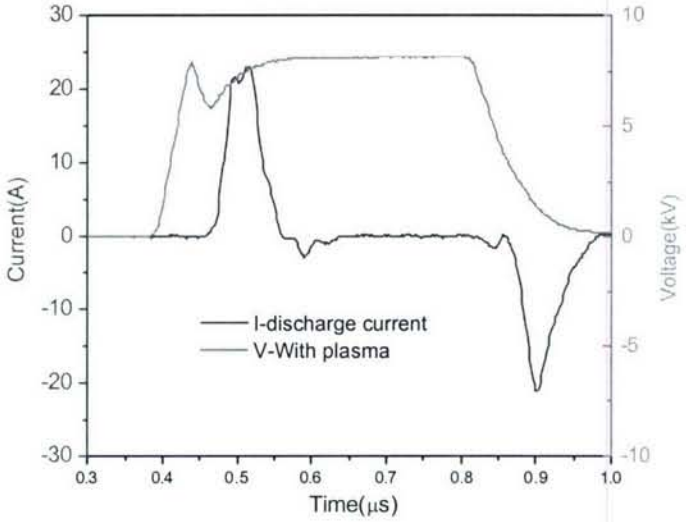

Fig. 17 The discharge current, I, is calculated from the total current minus the displacement current. The positive discharge current pulse is caused by the applied high voltage, which induces the breakdown of the gas gap. The negative discharge current pulse is caused by the charges deposited on the surface of the alumina plate.

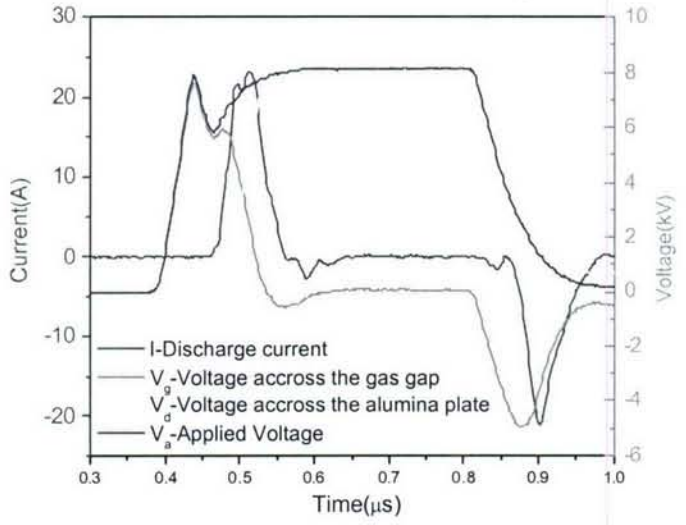

Fig. 18 Discharge current I, applied voltage V_a and calculated voltage across the gas gap,V_g ,and alumina plate,V_d. ($V_a=V_g+V_d$, $V_d = \frac{\int idt}{C_d}$, the capacitance of the dielectric plate is C_d=140pF).

Figure 18 shows that before the ignition of the discharge, the voltage across the gas gap is equal to the applied voltage. When the discharge starts, V_g decreases and V_d increases. This is because of the charges deposited on the alumina surface. When the applied voltage falls, the

negative voltage across the gas gap is caused by the charges deposited during the first current pulse. When this voltage reaches a certain value, it induces another discharge. Therefore two discharges (a **primary** discharge at the rising front of the voltage pulse and a **secondary** discharge at the falling front) are ignited for each voltage pulse. The secondary discharge does not consume any power from the power supply but is completely induced by charge storage during the initial discharge. This interesting phenomenon leads to increased power efficiency. Increasing the repetition rate of the applied voltage pulses will further enhance the plasma uniformity and stability since the double discharges per pulse will occur at a greater frequency.

Gas temperature measurements

The gas temperature can be estimated by analyzing the rotational structure of the N_2 second positive system emission. This rotational structure contains information on the rotational temperature. Because of the low energies needed for rotational excitation and the short transition times, molecules in the rotational states and the neutral gas molecules are in equilibrium. Therefore, the gas temperature can be directly inferred from the rotational temperature. To determine the gas temperature, we compared the experimentally measured spectra with simulated spectra of the 0-0 band of the second positive system of nitrogen. Fig. 19 shows the experimental measurement and simulated results with different gas temperatures. The curves are intentionally shifted vertically for better separation. For a gas temperature of 350K (green curve), the simulation results show that the rotational band stops at about 334.2nm (as shown by the arrow), this is approximately the same as our experimental results. In contrast for a temperature of 500 K the rotational bands extend to below 332 nm (blue curve). Therefore the gas temperature in our plasma is about 350K.

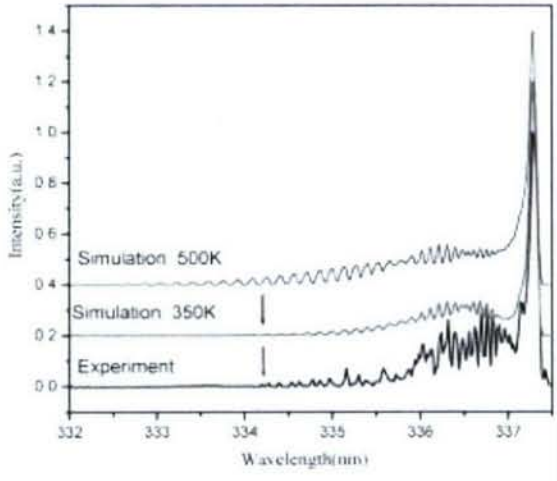

Fig. 19 Experimental and simulated spectra of N_2 second positive 0-0 transition. The applied voltage 9kV, pulse frequency 1kHz, pulse width 500ns, gap distance 2mm, background gas: $He+N_2(10\%)+Air(<1\%)$.

Emission Spectroscopy of the Pulsed Plasma

In order to identify and have a qualitative assessment of the species generated by the pulsed discharge under various gas mixtures, optical emission spectroscopy was applied. Figure 19 shows an example of emitted spectra between 200 and 500 nm when a mixture of helium, nitrogen, and air were used. The spectra are dominated by NO emission in the UV and by the second positive system of nitrogen for wavelengths greater than 300 nm.

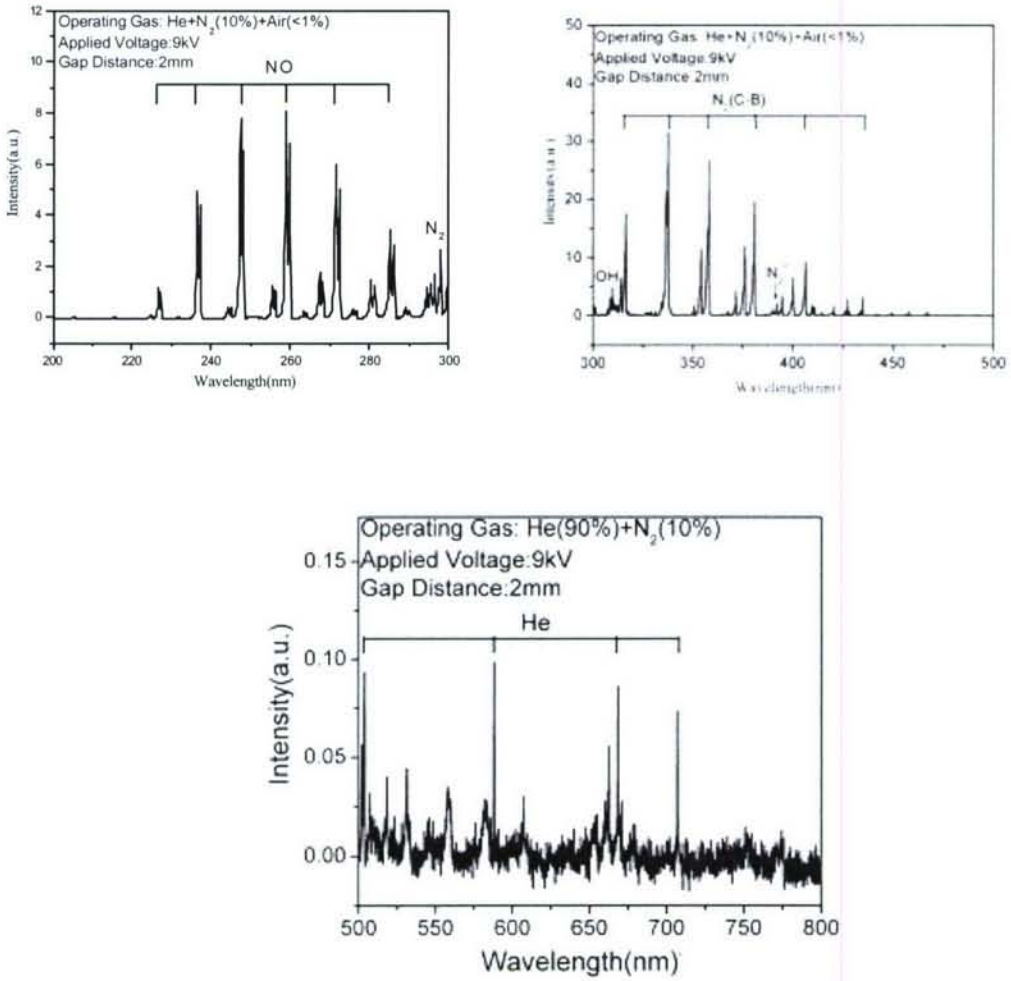

Fig. 19 Emission spectra from a pulsed He+N_2 plasma

Varying the percentages of He and N_2 we observed similar emission spectra but with weaker intensities. Spectra in the wavelength range 300nm-800nm (See Figs. 19) reveal the presence of excited OH, N_2, N_2^+, and He in the plasma.

Fast Photography: Discharge Structure

Because of its ability to capture the evolution of the discharge at time scales shorter than the characteristics times of most physical processes of interest, high-speed photography is a very useful tool that allows for a better understanding of the dynamics of the various discharge mechanisms. In the following, a high-speed ICCD camera with exposure time of 5ns is used to capture the temporal emission behavior of the primary and secondary discharges of the pulsed DBD. Figures 21 and 22 show the temporally and spatially resolved emissions of these two discharges. In these photos, on the far left is the copper disk electrode and on the far right is the alumina (Al_2O_3) covered electrode. The latter is connected to the high voltage while the former is directly connected to ground.

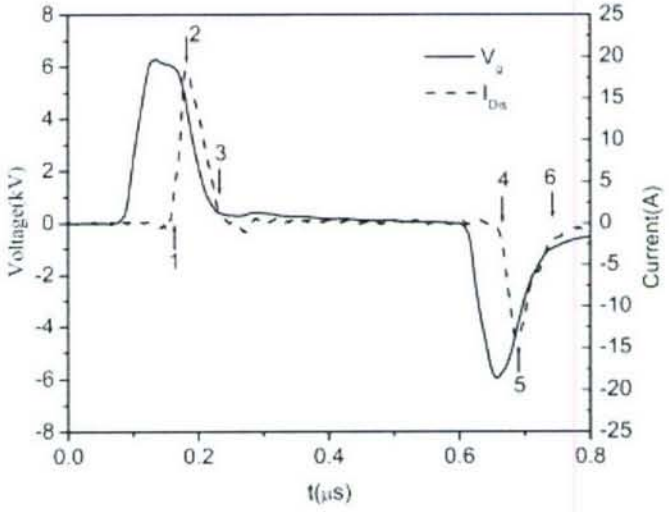

Fig. 20 I-V Characteristics

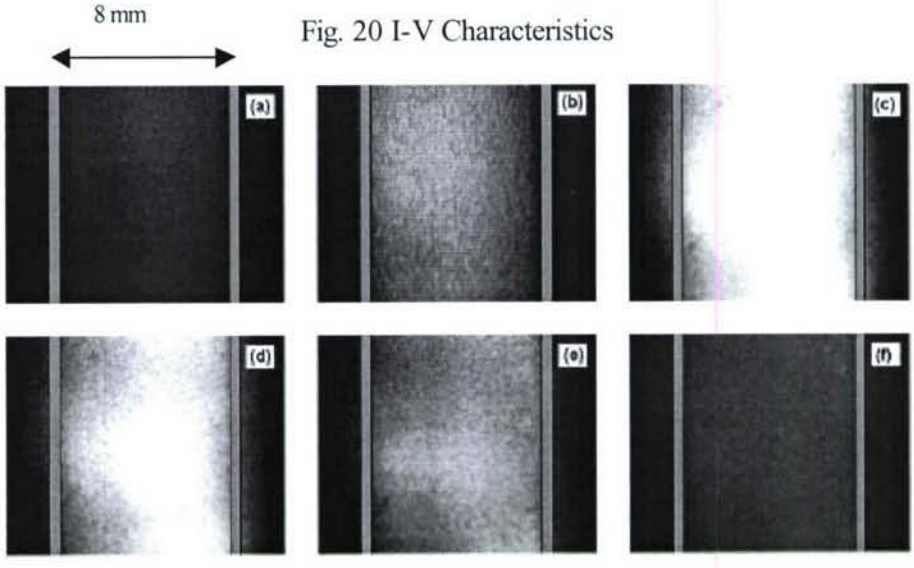

Fig. 21 ICCD pictures of the primary discharge. Exposure time is 5ns

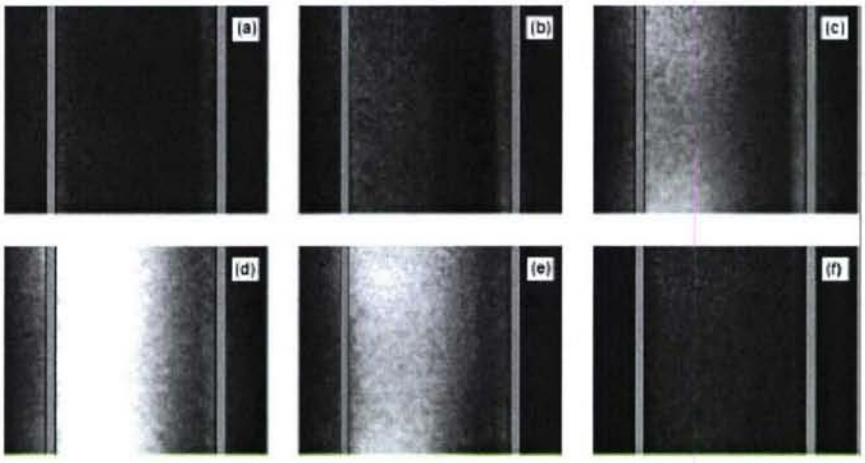

Fig. 22 ICCD pictures of the secondary discharge. Exposure time is 5 ns

At point 1 in Fig. 20, the voltage across the gap V_{gap} reaches its positive peak value, but the discharge current is zero. Figure 21(a) shows the emission at that moment. There is a weak emission from the gap. Since there is no discharge current, the detected light is emitted by the excited species left from the previous pulse. After 5ns, the discharge current I_{Dis} increases rapidly. Accordingly, Fig. 21(b) shows that the whole gap becomes brighter. After 20ns, I_{Dis} reaches its peak value as marked by point 2 in Fig. 20. The plasma emission at this time reaches its highest intensity as shown in Fig. 21(c). Then, when the discharge current decreases, the emission intensity decreases. This is illustrated by Figs. 21(d) and (e). After 70ns, which corresponds to point 3 in Fig. 20, the plasma emission becomes quite weak (see Fig. 21(f)) as the current decreases to almost zero. During the period between point 3 and point 4, there is no discharge current. Therefore the emission intensity from the bulk of the gap quickly decreases, except for the layers next to both electrodes, the intensity of which decreases at a slower rate.

Until point 4 in Fig. 20, the voltage across the gap reaches its negative peak value although no discharge current is established yet. Correspondingly, the plasma emission at that moment, shown in Fig.22(a), is very week with slightly higher emission from the two layers next to both electrodes. 5ns after the current begins to increase, the emission intensity increases and propagates from the left electrode (copper electrode) towards the right electrode (Aluminum covered with Al_2O_3) as shown in Fig.22(b). It is important to note that during this period the voltage pulse across the gap reverses (negative pulse), making the copper electrode (on the left) the anode. As the discharge current rises, the plasma emission intensity from the left electrode increases and rapidly expands towards the right side. The intensity from the layer next to the right electrode does not show any apparent change. When the discharge current reaches its maximum at point 5 (Fig. 20), Fig. 22(d) shows that the corresponding emission intensity reaches its maximum. The left side of the gap provides the strongest emission at this time. However, it should be pointed out that there is a dark space between the left strong emission area and the weak emission layer next to the right electrode. After point 5, the current starts to decrease, and so does the emission intensity. At point 6, as the current is close to zero, the emission intensity from the gap becomes weak again as illustrated by Fig. 22(f).

Summary and discussion:

For diffuse atmospheric pressure glow-like discharges (APGD) driven by AC power supplies, the typical discharge peak current is in the tens of mA range with a typical peak current density of few mA/cm^2. The typical discharge peak current and current density for a Townsend-like discharge (TD) are several to ten times less than that of glow-like discharges. However, as shown in Fig. 20, our discharge peak current is about 18A with a corresponding current density of $0.7A/cm^2$. These are two to three orders of magnitude higher than that of the classical AC-driven diffuse APGDs. We attribute this substantial increase to the fast rise and fall times of the applied voltage pulse, which results in a high reduced electric field. It is about 160Td in our case, which is about three to five times higher than that of traditional APGD in this kind of gas mixture.

Figure 20 shows that both the primary discharge current and the secondary discharge current last about 70ns. This time scale is close to that of filamentary discharges but much shorter than that of AC-driven APGDs. To have a better understanding of this phenomenon, the time t_e for an electron to travel from one electrode to the second electrode in pure He and N_2 is estimated. The products of pressure p and mobility of electron μ_e in pure He and N_2 are $0.86\times10^6 \ cm^2 \cdot Torr/V \cdot s$ and $0.45\times10^6 \ cm^2 \cdot Torr/V \cdot s$, respectively. For our case, under atmospheric pressure, the pressure p is 760Torr, the applied voltage V_a is 6kV and the gap distance d is 5mm. So the time t_e can be estimated by $t_e = d^2/\mu_e V_a$. These are 36 ns and 71 ns for pure He and N_2, respectively. This time scale is of the order of magnitude of the duration of the measured discharge current pulses. This correlation between the electrons transit time and the discharge current duration can be explained as follows: every time the discharge re-ignites, the electrons left in the bulk of the gap (from the prior discharge) and those close to the cathode region start moving towards the anode. During this process, the electrons excite, ionize and dissociate molecules and atoms. The electrons that start from the bulk of the gap reach the anode first. At this time, the discharge is in the self-sustained mode. But by the time the electrons originating from the cathode region reach the anode, the voltage across the gas gap falls below the ignition threshold and the discharge extinguishes. This is clearly evidenced by the decline of the current pulse observed in the I-V characteristics.

As mentioned above, the first discharge starts when the voltage across the gap reaches its maximum. It only takes about 20ns for the discharge current, as well as the emission intensity to reach their peaks. This process is much faster than that of atmospheric pressure glow discharges driven by AC voltages, which takes few micro seconds or longer.

It is noteworthy that the primary discharge starts from the volume of the gap and the whole volume becomes very bright when the current reaches peak. This is different than the normal glow discharge or Townsend discharge, which have a bright area next to the cathode or the anode, respectively.

The secondary discharge exhibits a very bright area next to the anode. This is similar with the Townsend discharge. However, the presence of a weak emission layer next to the cathode is not a typical feature in a Townsend discharge. Also, the secondary discharge appears more uniform than the primary discharge. This may be explained by the following reasons:

(1) Because the pulse repetition rate is 2 kHz, the time between the first discharge and the previous pulse is about 0.5 ms. On the other hand, there are only about 500 ns

between the secondary discharge and the primary discharge. So the concentrations of electron, ions and metastable species are much higher when the secondary discharge ignites. In addition, the week emission layers next to both electrodes may help the discharge to be more uniform.

(2) The lifetime of N_2 $B^3\prod_g$, $B'^3\Sigma_u^-$, $a''^1\Sigma_g^+$, and $D^3\Sigma_u^+$ states and N_2^+ $A^2\prod_u$ states are in the microsecond and sub-microsecond ranges. These states may contribute to the secondary discharge, but not the primary discharge since their lifetime is too short compared to the time between pulses. However, some of the metastable states may have much longer lifetimes and may contribute to both the primary discharge and secondary discharge, such as N_2 $A^3\Sigma_u^+$ state, which has a lifetime of more than one second. The N_2 $a^1\prod_g$ state, which has a lifetime of sub-millisecond and can result in stepwise ionization, is also believed to be involved in both discharges.

B. A Novel Cold Plasma Plume for Biomedical Applications: The Plasma Pencil

During this period of performance we have developed a novel atmospheric pressure cold plasma generators that is suitable for localized treatment of biological objects. This device which we call "plasma pencil" is capable of generating a long cold plasma plume in the surrounding room air. The way it operates is as follows.

Device Description

Sub-microsecond high voltage pulses at repetition rates in the 1-10 kHz range are applied between two specially designed electrodes through which helium gas is flowing (flow rates in the 1-10 liter/min range). Each of the two electrodes is made of a thin copper ring attached to the surface of a centrally perforated glass disk. The hole in the center of the glass disk is about 3 mm in diameter, while the diameter of the disk is about 2.5 cm. The diameter of the copper ring is greater than that of the hole but smaller than that of the disk. The two electrodes are inserted in a dielectric cylindrical tube of about the same diameter as the glass disks and are separated by a gap the distance of which can be varied in the 0.5-1 cm range. Figure 23 is a schematic of the device. When helium is injected at the opposite end of the dielectric tube and the high voltage pulses are applied to the electrodes, a discharge is ignited in the gap between the electrodes and a plasma plume reaching lengths up to 5 cm is launched through the hole of the outer electrode and in the surrounding room air. Figure 24 is a photograph of the plasma plume. The length of the plume depends on the helium flow rate and the magnitude of the applied voltage pulses. The plasma plume remains at low temperature and can be touched by bare hands without any harm. The device, being basically a 1inch diameter dielectric tube (about 5 inches long) can be hand held and the plume directed at will towards a surface to be treated including human skin or dental gums. Unlike other known plasma "jet" devices, which generate very short plumes in the millimeter range, and at temperatures that can reach several tens of degrees above room temperature, this device is capable of producing and maintaining room temperature plasma plumes more than an order of magnitude in size. Also unlike corona-like devices such as the plasma needle, which generates 2-3 mm long plasma at the tip of a sharp wire (needle), this

device contains no sharp metal objects and since narrow sub-microsecond voltage pulses are used, as opposed to RF power, the risk of arcing and device heating for long operation periods (hours) is avoided.

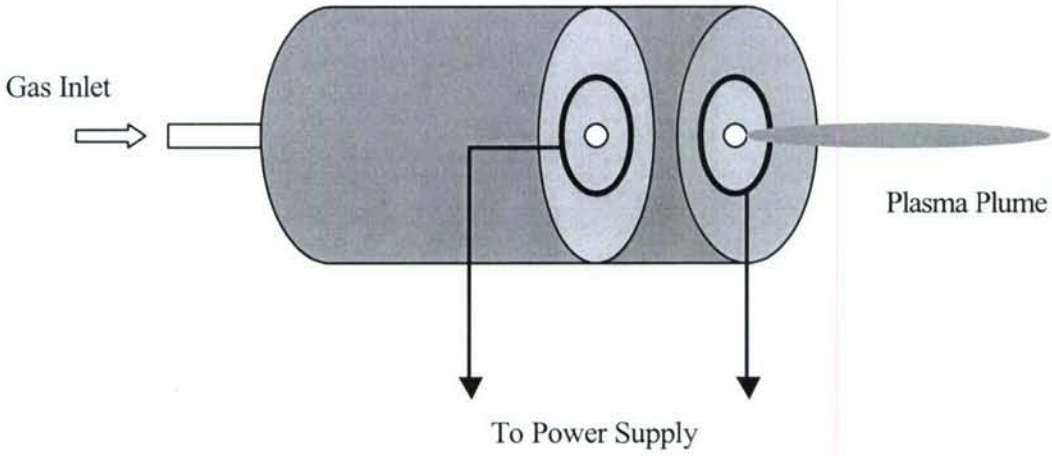

Fig. 23 Schematic of the "Plasma Pencil"

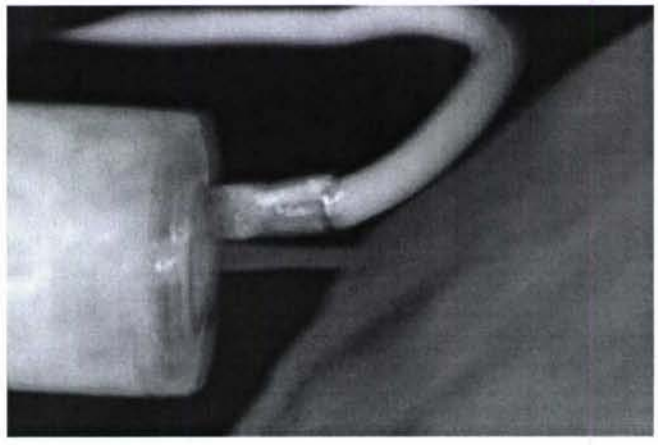

Fig. 24 Plasma pencil showing plume in contact with the PI's hand

Current-voltage Characteristics

For all the experimental results presented here the operating gas was helium, the applied voltage, pulse width, pulse frequency and gap distance were V_a = 5 kV, t_{PW} = 500 ns, f = 1khz, and d = 5mm, respectively. The helium gas flow rate was 3.5 l/min.

The current-voltage characteristics of the discharge are shown in Figure 25 and Figure 26. Figure 25 shows the applied voltage V_a, displacement current I_{no} (without He flow: no plasma) and total current I_{ot} (with plasma on). It should be mentioned that the voltage waveform remains the same when the plasma is on or off. To find out the actual discharge current, the displacement current I_{no} is subtracted from the total current I_{tot}. Figure26 shows the applied

voltage V_a and actual discharge current I_{Dis} versus time. The first pulse of the discharge current starts after the applied voltage reaches its plateau value. The delay between the start of the applied voltage and that of the first discharge current pulse is about 60 ns. The first current pulse (between point 1 and 3) lasts about 100ns. Immediately after the first current pulse, the discharge current has another increase. The peak value of this second current pulse is about one fourth that of the first current pulse. But it lasts much longer (between point 3 and 6), about 375 ns. As can be seen, this second current pulse rises to a peak value of about 1.2 A in 100ns (between point 3 and 4), then slowly decreases to zero in 275ns (between point 4 and 6). It is interesting to note that this second current pulse was not observed in our planar dielectric barrier discharge driven by the same power supply (this particular device did not emit a plume). The mechanism of this second current pulse, which is directly linked to the launch of the plume, will be discussed in the next section. After point 6, which is about 25 ns after the arrival of the falling front of the applied voltage (point 5), a third current pulse starts. This corresponds to a new breakdown of the gap. This discharge ignites because of the voltage induced by the charges, which have accumulated on the surface of the dielectric disk during the previous discharge. This current pulse lasts about 100ns then decays to zero.

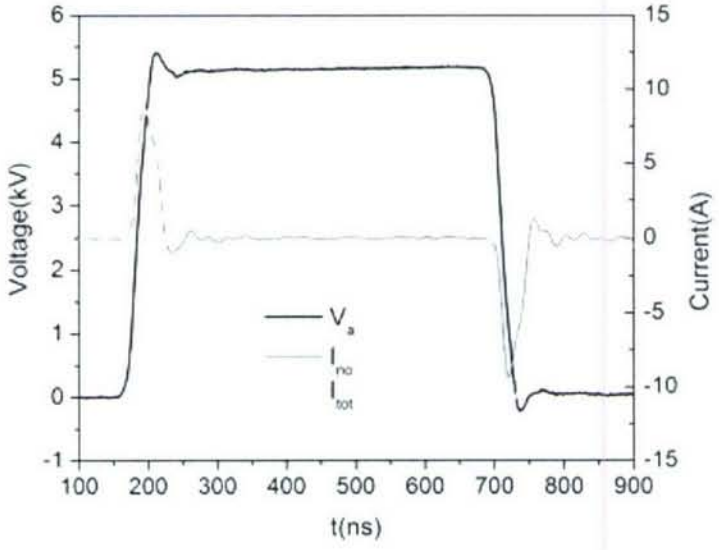

Fig. 25 I-V Characteristics showing the current with the plasmas off as well as the total current

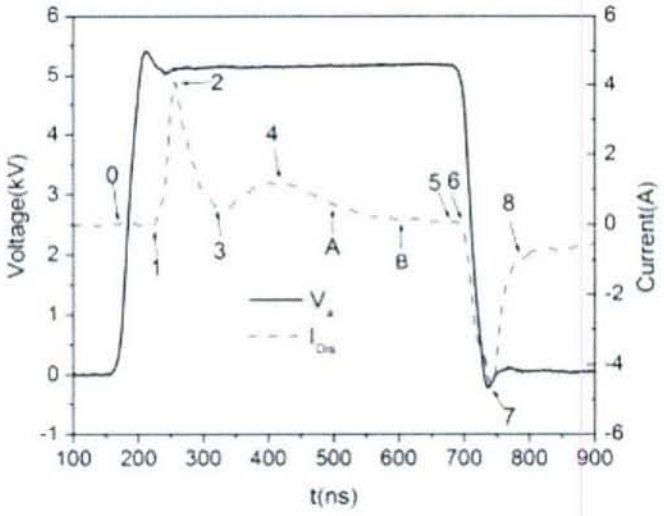

Fig. 26 I-V Characteristics showing the actual discharge current

Emission Spectra

To identify the various reactive species generated by the plasma plume, optical emission spectroscopy (OES) is applied in the 200-800 nm wavelength range. For this task a half-meter spectrometer (Acton Research SpectraPro 500i) equipped with a photomultiplier (Hamamatsu R928) is used. No line emission was detected in the 200-280 nm range. Figures 27 shows that the emission spectra are dominated by the presence of excited nitrogen, helium, and nitrogen ions. In addition highly reactive radicals such as hydroxyl (OH) and atomic oxygen are detected. These radicals play important roles in all plasma-surface interactions. Their highly oxidative nature allows them to change important surface properties such as hydrophobicity. Their contact with organic matter (such as cells) leads to interesting processes such as oxidation of membrane lipids and proteins. In the case of bacteria (prokaryotes) this oxidation can lead to cell inactivation and even to cell lysis. In the case of mammalian cells (eukaryotes), other processes such cell detachment or cell apoptosis can result.

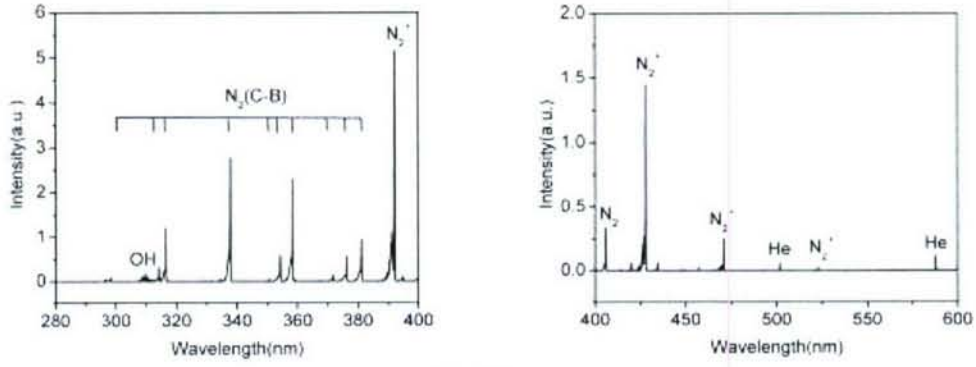

Fig. 27

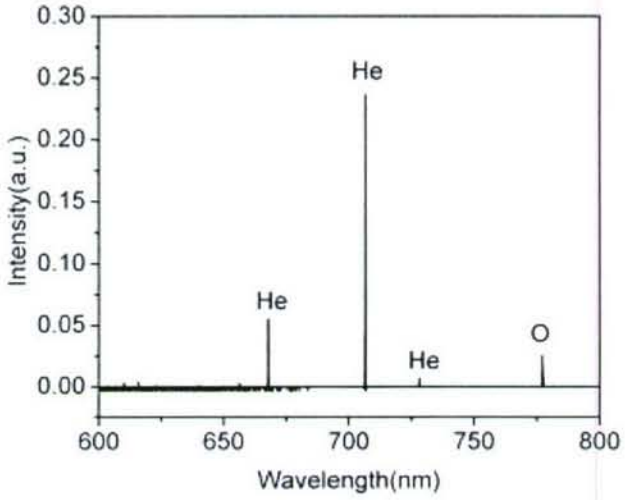

Fig. 27 (continue) Emission spectra

Fast Photography: Discharge structure

As we reported earlier, the plasma plume can achieve lengths of up to 5 cm. To better understand the dynamics of the plasma plume, a high-speed ICCD camera with an exposure time of 50 ns is used to capture the temporal emission behavior of the plasma. Figure 28 shows that the plume is actually a small volume of plasma traveling at a very high velocity. This bullet-like plasma is launched from the exit aperture of the device and into open air. Its velocity, in the order of 10^5 m/s is far higher than the gas velocity which only about 8 m/s. We believe that photo-ionization plays an important role in the propagation of the plasma bullet. Figure 29 is a plot of the plume velocity as a function of time (at 320 ns the plasma bullet is just exiting the device).

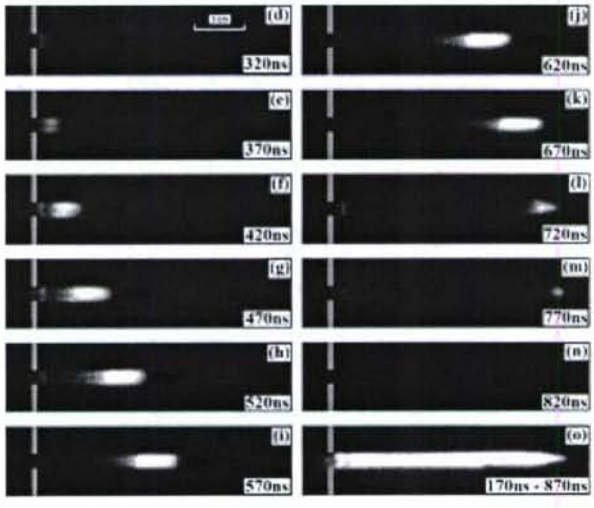

Fig. 28 ICCD pictures of the plasma plume

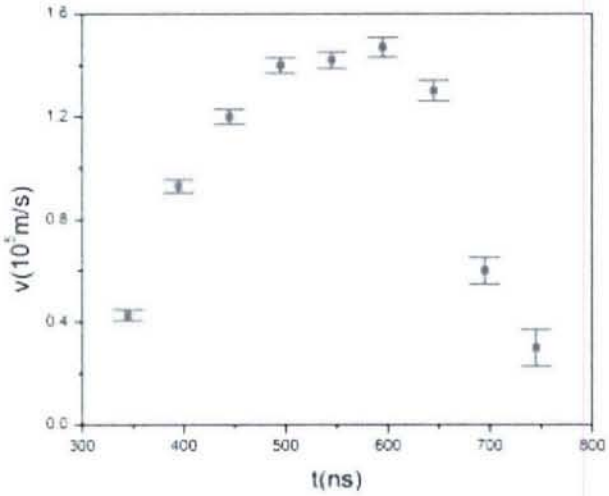

Fig. 29 Plume velocity versus time

Biological Applications

As low temperature non-equilibrium plasmas come to play an increasing role in biomedical applications, reliable and user-friendly sources need to be developed. These plasma sources have to meet stringent requirements such as low temperature (at or near room temperature), no risk of arcing, operation at atmospheric pressure, portability, optional hand-held operation, etc. The plasma pencil meets these requirements. This device is capable of generating a cold plasma plume several centimeters in length. It exhibits low power requirements (1–3 W) as shown by its current voltage characteristics. Using helium as the main component of the operating gas the plasma temperature (heavy species, i.e. neutrals, ions), as measured by both emission spectroscopy and with an infrared detector, is and remains at room temperature. The plasma plume can be directed manually by a user to come in contact with delicate objects and materials including skin and dental gum without causing any heating or painful sensation.

Various bacteria were inactivated by the plasma pencil, however, it was found that in general gram-negative bacteria were more susceptible to be inactivated by the plasma plume. Figure 30 shows an example for *E. coli*. It illustrates that the treatment is localized, which can be desirable in some situations, and effective. The plume was aimed at the center of the Petri dishes, as shown in Figure 31. The affected area (dark zone in the middle) in this case is a well-defined zone where no growth occurs after a period of incubation. In the case of other bacteria the treated area was more or less well defined depending on the initial concentration used.

Fig. 30 Photographs of petri dishes showing the effects of the cold plume, generated by the plasma pencil, on *E.coli* cells. Operating gas is helium. Top petri dish is control, bottom petri dishes were treated for 30 seconds (left) and 120 seconds (right).

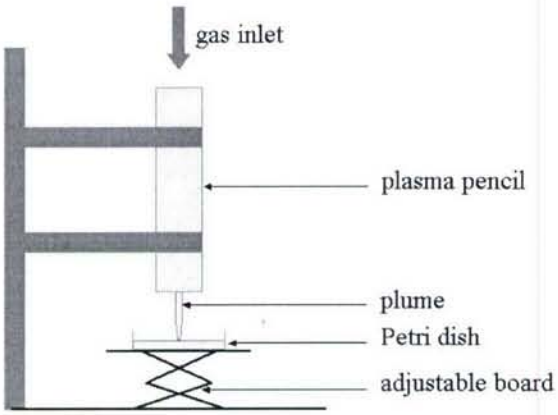

Fig. 31 Experimental setup

Other Activities of the P.I.

In the duration of this research program the principal Investigator was involved in various other research and scholarly activities. In collaboration with Microenergy Technologies Inc., the PI and his group conducted investigations on the effects of air plasmas on the cells of

microorganisms. This work has direct applications of interest to the Air Force. Examples are the rapid sterilization of medical tools and the biological decontamination of equipment and gears. The PI and his research group have also continued their contributions to another research program of interest to the Air Force. This relates to the design of compact pulsed power systems. Our work focused on the use of liquids (such as water) as a switching medium and on the hold-off capability of liquid-based systems. This work was supported by an AFOSR MURI on "Compact Portable Pulsed Power".

The PI got involved in various other scholarly activities. In 2004 he gave a plenary lecture at the IEEE Int. Conference on Plasma Science and was the minicourse organizer at that conference. He organized oral and poster sessions at the 2005 IEEE International Conference on Plasma Science, Monterey, CA. He also was the general Co-Chair of the Fourth Electromed Conference, which took place in Portland, OR, May 16-18, 2005. In May, 2005 the PI gave an invited lecture at the Institute of Physics, London, UK, titled "Low Temperature Plasmas in Biotechnology". The PI, who served on the Administrative Committee of the IEEE Nuclear and Plasma Science Society, was elected to a three-year term (2005-2007) as member of the Executive Committee of NPSS PSAC. In 2006 the PI gave two invited talks, one at the Gaseous Electronics Conference, and the second at the IEEE Int. Conf. on Plasma Science.

Publications

2003-2004

M. Laroussi, D. A. Mendis, and M. Rosenberg, "Plasma Interaction with Microbes", *New Journal of Physics*, Vol. 5, pp. 41.1-41.10, 2003.

X. Lu, F. Leipold, and M. Laroussi, "Optical and Electrical Diagnostics of a Non-equilibrium Air Plasma", *J. Phys. D: Appl. Phys.*, Vol. 36, pp. 2662-2666, 3003.

M. Laroussi and F. Leipold, " Evaluation of the Roles of Reactive Species, Heat, and UV radiation in the Inactivation of bacterial Cells by Air Plasmas at Atmospheric Pressure", *Int. J. Mass Spectrom.*, Vol. 233, pp. 81-86, 2004.

J. A. Gaudet, R. J. Barker, C. J. Buchenauer, C. Christodoulou, J. Dickens, M. Gundersen, R. P. Joshi, H. G. Krompholz, F. F. Kolb, A. Kuthi, M. Laroussi, A. Neuber, W. Nunnaly, E. Schamiloglu, K. H. Schoenbach, J. S. Tyo, and R. Vidmar, " Research Issues in Developing Compact Pulsed Power for High Peak Power Applications on Mobile Platforms", *Proceedings of the IEEE*, Vol. 92, No. 7, pp. 1144-1165, 2004.

X. Lu, F. Leipold, O. Minayeva, and M. Laroussi, "Non-thermal Air Plasma at Atmospheric Pressure", *In Proc. Gaseous Electronics Conf.*, p.53, San Francisco, CA 2003.

S. Xiao, J. F. Kolb, C. Bickes, Y. Minamitani, M. Laroussi, K. H. Schoenbach, and R. Joshi, "Recovery of High Power Switches", *In Proc. 26th Power Modulator Conference*, San Francisco, CA, p. 39, May 23-26, 2004.

J. F. Kolb, X. Lu, S. Xiao, C. Bickes, Y. Minamitani, M. Laroussi, K. H. Schoenbach, R. Joshi, and E. Schamiloglu, "Electrical Breakdown in Polar Liquids", *In Proc. 26th Power Modulator Conference*, San Francisco, CA, p. 121, May 23-26, 2004.

Y. Minamitani, B. Goan, J. F. Kolb, S. Xiao, , C. Bickes, X. Lu, M. Laroussi, K. H. Schoenbach, S. Kono, and R. Joshi, "Transient Interferometric Measurements of Electric Field and Temperature Distributions in Pulse Discharged Water Gaps", *In Proc. 26th Power Modulator Conference*, san Francisco, CA, p. 142, May 23-26, 2004.

O. Minayeva and M. Laroussi, "Molecular Absorption Spectroscopy of the Atmospheric Pressure Air DBD", *In Proc. IEEE Int. Conf. Plasma Sci.*, Baltimore, MD, p. 122, June 28-July 1, 2004.

M. Laroussi, X. Lu, V. Kolobov, and R. Arslanbekov, "Pulsed DBD at Atmospheric Pressure", *In Proc. IEEE Int. Conf. Plasma Sci.*, Baltimore, MD, p. 228, June 28-July 1, 2004.

J. F. Kolb, Y. Minamitani, S. Xiao, S. Kono, B. Goan, X. Lu, J. Qian, M. Laroussi, R. Joshi, K. H. Schoenbach, , and E. Schamiloglu, "Electrical Breakdown in Polar Liquids", *In Proc. IEEE Int. Conf. Plasma Sci.*, Baltimore, MD, p. 271, June 28-July 1, 2004.

J. F. Kolb, S. Xiao, B. Goan, X. Lu, K. H. Schoenbach, M. Laroussi, R. Joshi, J. Dickens, A. Neuber, H. Krompholz, M. Cevallos, and M. Butcher, " Nanosecond Optical Diagnostics for Liquid Dielectric Switches", *In Proc. IEEE Int. Conf. Plasma Sci.*, Baltimore, MD, p. 402, June 28-July 1, 2004.

M. Laroussi, " Non-Equilibrium Plasma-based Sterilization: Overview, State-of-the art, and Challenges", *In Proc. IEEE Int. Conf. Plasma Sci.*, Baltimore, MD, p. 107, June 28-July 1, 2004

2005

M. Laroussi, "Low Temperature Plasma-Based Sterilization: Overview and State-of-the-Art", *Plasma Proc. Polym.*, Vol. 2, No. 5, pp. 391-400, 2005. **Feature paper.**

X. Lu and M. Laroussi, "Atmospheric Pressure Glow Discharge in Air Using a Water Electrode", *IEEE Trans. Plasma Sci.*, Vol. 33, No. 2, pp. 272-273, 2005.

X. Lu and M. Laroussi, " Optimization of ultraviolet emission and chemical species generation from a pulsed dielectric barrier discharge at atmospheric pressure", *J. Appl. Phys.*, Vol. 98, 2005.

M. Laroussi and F. C. Dobbs, "Inactivation of Bacteria by Plasma-Generated Incoherent Excimer UV Radiation", *In Proc. Electromed05*, Portland, OR, pp. 42-46, 2005.

X. Lu and M. Laroussi, "Experimental Studies on a sub.microsecond Pulsed Dieletric barrier Discharge at Atmospheric Pressure", In Proc. Int. Symp. Plasma Chem., Toronto, Canada, August 2005.

J. Kolb, Y. Minamittani, S. Xiao, M. Laroussi, R. P. Joshi, K. H. Schoenbach, E. Schamiloglu, and J. Gaudet, "The Permettivity of Water Under High Dielectric Strength", In Proc. Pulsed Power Conf., Monterey, CA, 2005, *In Press*.

X. Lu, J. Kolb, S. Xiao, M. Laroussi, K. H. Schoenbach, and E. Schamiloglu, "Dielectric Strength of Sub-millimeter Water gaps Subjected to Microsecond and Sub-microsecond Voltage Pulses", In Proc. Pulsed Power Conf., Monterey, CA, 2005, *In Press*.

O. Minayeva, J. Wood, F. C. Dobbs, and M. Laroussi, "Remote Plasma Treatment of bacteria Using Non-equilibrium Atmospheric Pressure Air Dielectric Barrier Discharge", *In Proc. IEEE Int. Conf. Plasma Sci.*, Monterey, CA, p. 151, 2005.

X. Lu and M. Laroussi, "Diagnostics of Non-equilibrium High Pressure Plasmas Generated by the Resistive barrier Discharge", *In Proc. IEEE Int. Conf. Plasma Sci.*, Monterey, CA, p. 227, 2005.

2006

X. Lu and M. Laroussi, "Temporal and Spatial Emission Behavior of Homogeneous Dielectric Barrier Discharge Driven by Unipolar Sub-microsecond Square Pulses", *J. Phys. D: Appl. Phys.* **39**, pp. 1127-1131, 2006.

M. Laroussi, C. Tendero, X. Lu, S. Alla, and W. L. Hynes, "Inactivation of bacteria by the Plasma Pencil", *Plasma Proc. Polym*.**3**, pp. 470-473, 2006.

M. Laroussi, O. Minayeva, F. C. Dobbs, and J. Woods, "Spores Survivability after Exposure to Low-Temperature Plasmas", *IEEE Trans. Plasma Sci.* Vol. 34, No. 4, 2006.

S Xiao, J. Kolb, A. Malik, X. Lu, M. Laroussi, R. Joshi, and K. Schoenbach, "Electrical Breakdown and Dielectric Recovery of Polar Liquids", *IEEE Trans. Plasma Sci.*, Vol. 34, No. 5, pp. 1653-1661, 2006.

X. Lu and M. Laroussi, "Dynamics of an Atmospheric Pressure Plasma Plume Generated by Submicrosecond Voltage Pulses", *J. Appl. Phys*. **100**, 2006.

X. Lu and M. Laroussi, "Homogeneous Dielectric Barrier Discharge Driven by Unipolar Sub-microsecond Square Pulses", *Int. Power Modulator Conf.*, p. 102, Washington DC, May 2006.

X. Lu, C. Tendero, and M. Laroussi, "The Plasma Pencil: A Novel Cold Plasma Source for Low Pressure Applications", *IEEE Int. Conf. Plasma Sci.*, p. 238, Traverse City, MI, June 2006

C. Tendero, X. Lu, S. Alla, W. Hynes, and M. Laroussi, "Effects of the Plasma Pencil on Different Bacteria Genera", *IEEE Int. Conf. Plasma Sci.*, p. 265, Traverse City, MI, June 2006. **Invited Paper.**

M. Laroussi, "Interaction of Non-equilibrium Plasmas with Biological Cells: What we have Learned so Far", *Gaseous Electronics Conf.*, Columbus, OH, Oct. 2006. **Invited Paper**

T. Akan, X. Lu, and M. Laroussi, "The Plasma Pencil: A Novel Pulsed Plasma Source", *Gaseous Electronics Conf.*, Columbus, OH, Oct. 2006.

Personnel

M. Laroussi, Old Dominion University, PI
Xinpei Lu, Old Dominion University
S. Reddy Alla, Master Student, Old Dominion University
Frank Leipold, Old Dominion University
Olga Minayeva, Old Dominion University